ACS OMEGA

Open Access

http://pubs.acs.org/journal/acsodf

Article

Fabrication and Characterization of Montmorillonite Clay/Agar-Based Magnetic Composite and Its Biological and Electrical Conductivity Evaluation

Nasrullah Shah,* Muffarih Shah, Farishta Khan, Touseef Rehan, Sulaiman Shams, Fatima Khitab, Abbas Khan, Muhammad Wajid Ullah, Jasim Yousaf, Fuad A. Awwad, and Emad A. A. Ismail

Cite This: *ACS Omega* 2024, 9, 15904−15914

Read Online

ACCESS | Metrics & More | Article Recommendations

ABSTRACT: Montmorillonite clay and agar are naturally occurring materials of significant importance in designing biocompatible materials tailored for applications in biotechnology and medicine. The introduction of magnetic properties has the potential to significantly boost their characteristics and expand their applications. In this study, we have successfully synthesized highly intercalated magnetic composites, incorporating magnetic iron oxide nanoparticles (MNPs), montmorillonite clay (MMT), and agar (AG), through a thermo-physicomechanical method. Three samples of MMT-AG with 2, 1.5, and 0.5% MNPs and three sample composites of MNPs-AG with 2, 1, and 0.5% MMT clay are prepared. The synthesized composites were characterized by SEM, XRD, TGA, DTA, and FTIR. SEM analysis revealed a uniform dispersion of MNPs and MMT in the composite. The XRD pattern confirmed the presence of MNPs in the composite site. The TGA and DTA results demonstrated improved thermal stability due to the MNP incorporation. FTIR spectra showed all of the constituents of agar, MNPs, and MMT clay. The swelling ratio was observed to range from 835% to 1739%. The swelling study indicated an increased hydrophobicity with the addition of MNPs to the composite. Antibacterial activities revealed a significant inhibition of *Escherichia coli* (*E. coli*) growth by ranging from 10 to 19 nm in the composite. The composite also exhibited a considerable antioxidant action, with IC50 values of 7.96, 46.55, and 57.58 μg/mL, and electrical properties just like conductors.

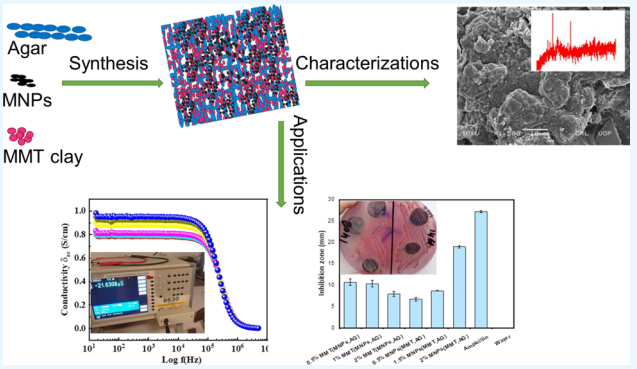

1. INTRODUCTION

Agar (AG) is a promising organic polymer owing to its excellent attributes such ecofriendliness, biocompatibility, biodegradability, cost-effectiveness, and scientific merits. It emerges as a prime polysaccharide for applications in biomedical engineering.[1,2] AG, a versatile biopolymer, can be derived from seaweed through an alkali treatment process or synthesized from fructose-6-phosphate. When mixed with water, it takes a jelly-like consistency. AG, along with its composites, has a range of applications in drug delivery, wound healing, tumor therapy, and hyperthermia treatment. Due to their ability to scatter sound waves, AG gel formulations are commonly used for ultrasound imaging. Researchers have also discovered that AG can act as a matrix for modified drug release. AG-based composites have been found to be effective in healing wounds, burns, and ulcers. Furthermore, AG can serve as a matrix for carbonyl iron, a material with excellent thermal conductivity, making it a valuable tool in hyperthermia treatments.[3−7]

However, AG-based materials exhibit certain shortcomings, including poor mechanical, optical, thermal, and antibacterial characteristics.[8] Additionally, they are brittle and have weak water-barrier qualities. Different strategies have been used to overcome these disadvantages. The physical characteristics of AG-based films are enhanced by the use of various fillers. In biopolymer-based nanocomposites, Montmorillonite (MMT) is a form of clay that is frequently utilized because of its swelling qualities, ability to store water between the layers of platelets, and ion-exchange capabilities.[9] Due to the substantial effects of their interactions on the properties of both the clay and the polymeric constituent, such clay-based composite

Received: November 2, 2023
Revised: February 22, 2024
Accepted: February 26, 2024
Published: March 31, 2024

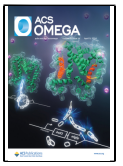

https://doi.org/10.1021/acsomega.3c08708
ACS Omega 2024, 9, 15904−15914

materials (conventional composites, intercalated composites, and exfoliated composites) have attracted a lot of research interest.[10,11] The mineral MMT, which belongs to the smectite group, has a layered structure.[12] Formation of MMT results from the weathering of eruptive rock materials. It is considered a valuable model for studying the properties of smectic clay minerals due to its high swelling capacity and ability to produce stable suspensions.[13] According to their ionic or nonionic nature, the polymers in the MMT dispersions interact with the clay particles. The nonionic polymers are adsorbed on the surface of clay minerals by the steric interactions, whereas the ionic polymers cause electrostatic interactions. The clay/polymer interactions may be influenced by the concentration of the polymer, the molecular weight and hydrolyzing groups of the polymer, the size and shape of the clay particle, its surface charge, the concentration of the clay in suspension, the pH, and the temperature. The rheological and electrokinetic characteristics of the system are affected by the adsorption of polymers onto the surfaces of clay particles.[12] In addition, the MMT-based composites are also well known for the long-term antimicrobial effect. Another way to minimize these limitations in AG-based composites is the addition of certain metallic nanoparticles such as magnetic nanoparticles (MNPs) into the polymer.[14] It imparts magnetic, thermal, and electrical properties to the composites.[15−17] MNPs have potential applications in bioimaging. Biocompatible coating of MNPs can be used due to their high surface-to-volume ratio and surface energy that may enhance their properties.[18−20]

To sum up, the nanoparticle's enhanced quality with MMT clay's compatibility and AG-based films, viability, economy, nontoxic nature, and its ability to improve the physical properties of composite films make it an ideal candidate for studies.[21−23] Several relevant research works within the same domain have been referenced here. Polat et al.[24] evaluated AG/k-carrageenan/montmorillonite hydrogel as a wound dressing. The hydrogels released analgesic lidocaine hydrochloride and antibiotic chloramphenicol drugs in a regulated manner and exhibited strong antibacterial activity against *E.coli* and *S. aureus*. According to Wu et al.,[25] flame-retardant polyamide 6/nanoclay/intumescent nanoparticle fibers were synthesized by electrospinning and using formic acid as a solvent. It is worth noting that only other studies employed solution compounding in the creation of nylon6/layered silicate nanocomposites. Paci et al.[26] also used formic acid to prepare nylon6/Cloisite 30B nanocomposites and found that a low filler content and small polymer/clay particles can lead to intercalation or even complete destruction of the silicate platelet stacking order. According to Filippi et al.,[27] composites of ethylene copolymers and organically modified montmorillonite cannot be intercalated through solution blending. Another study on the synthesis and characterization of chitosan−MMT biocomposite conducted by Günister et al.[12] investigated the rheological behaviors and colloidal properties of the clay dispersions as well as the chitosan−MMT biocomposite system. New nanocomposite films for food packaging were developed by Lee et al.[9] using agar, Gellan gum, and MMT clay. The addition of clay improved the thermal stability and tensile strength but reduced the water barrier and contact angle.

Performance of such biopolymer/clay nanocomposites is affected by a variety of parameters, including the polymer matrix compatibility and the kind of nanoclays used,[28] nanocomposite production methodology,[29] and contents of the nanoclay.[30] Therefore, it is very important to test the effect of the clay content to determine the optimal nanoclay quantity for preparing nanocomposite films with the necessary film characteristics for the packaging applications. There are many methods of composite preparations including the solution casting method,[31] melt mixing process,[32] in situ method,[33] compression molding method,[34] extrusion method,[34] resin transfer molding,[35] and so forth.

These hybrid materials have potential applications in environmental remediation,[36] drug loading and release,[37,38] cancer therapy,[39] antimicrobial activities,[40] antifungal activities,[41] antioxidant actions,[42] dye adsorption,[43] wound dressing,[44] bone tissue engineering,[45] food packing and safety,[44] electromagnetic shielding,[46] magnetic sensing,[47] electrochemical properties,[45] oil−water separation,[48] and electronic devices.[49]

The current work focuses on the synthesis, characterization, swelling behavior studies, electrical conductivity tests, and antioxidant and antimicrobial activities of MMT clay-based magnetic AG composites. Selection of this work was motivated by the combination of characteristics, including thermal and mechanical stabilities and cost-effectiveness, as compared to the already reposted (clay, MNPs, and agar with other materials) composites.

2. EXPERIMENTAL SECTION

2.1. Chemicals and Reagents. All of the chemicals used were of analytical grade. AG and MMT clay powder were from DAEJUNG Chemicals and Metals CO., LTD., Korea. $FeCl_2.4H_2O$, $FeCl_3.6H_2O$ (Riedel-de Haem, Germany), hydrochloric acid (HCl), 2, 2-diphenylpicrylhydrazyl (DPPH), and sodium hydroxide (NaOH) were obtained from Riedel-de-Haem, Germany. Bacterial strains were offered by the Department of Biochemistry, AWKUM.

2.2. Instrumentation. A Fourier transform infrared spectrometer (Nicolet iS5), a scanning electronic microscope (SEM) (Joel JSM5910, Japan), a thermogravimetric analyzer (PerkinElmer, USA), and an X-ray diffractometer (D-2 Phase, Bruker, Denver, CO, USA) at a scanning rate of 20 °C/min with copper kα radiation were used for various analysis.

2.3. Preparation of Magnetic Iron Oxide Nanoparticles. A 0.4 g portion of $FeCl_3.6H_20$ and 4g of $FeCl_2.4H_2O$ were dissolved in 50 mL of deoxygenated water and 1.7 mL of concentrated HCl. The mixture was then added into 250 mL of 1.5 M NaOH solution. Fe_3O_4 (MNPs) are not very stable, and they can be oxidized into Fe_2O_3 in the presence of oxygen. To prevent this oxidation in air, an oxygen-free environment is very important. Nitrogen is used to produce such an environment by passing through the solution. Nitrogen gas through the solution not only can prevent the oxidation but also reduces the particle size. The solution is then stirred and purged with N_2 gas until the temperature reached 373 °F under a nonoxidizing, oxygen-free environment[50] The product was collected by an external magnetic field and rinsed with deionized water three times, and dried in a vacuum at 80 °C for an hour to obtain MNPs.[51]

2.4. Preparation of MNPs (MMT and AG) Magnetic Composite Sheets. For the preparation of different percentage amounts of iron oxide nanoparticles (NPs), i.e., 0.5, 1.5, and 2% in the MMT and AG magnetic composite, a simple thermo-physicomechanical method was used. 0.5 g of AG was taken in a flask with 50 mL of distilled water and placed on a hot plate. 1 g of pure MMT clay was taken in 30

https://doi.org/10.1021/acsomega.3c08708
ACS Omega 2024, 9, 15904−15914

mL of distilled water and sonicated for 5 min before adding to an AG solution and shaken well for about 5 min prior to its heating. Then, the sonicate suspension of 0.5 g of MNPs in 20 mL of distilled water was added to the AG and MMT solution and heated up to 90 °C for 30 min. The solution condensed. This condensed solution was then poured into a Petri dish and solidified at room temperature. This solidified composite was placed in sunlight for complete drying. The same method was used for the preparation of 1.5 and 2% MNP (MMT and AG) magnetic composite sheets.

2.5. Preparation of MMT (MNPs and AG) Magnetic Composite Sheets. For the preparation of different percentages of MMT clay, i.e., 0.5, 1, and 2%, in the iron oxide nanoparticles and AG magnetic composite, a simple thermo-physicomechanical method was used. 0.5 g of AG was taken in a flask with 50 mL of distilled water placed on a hot plate. 0.5 g of pure MMT clay was taken in 30 mL of distilled water and sonicated for 5 min before adding to the AG solution shaken well for about 5 min prior to its heating. Then, the sonicate suspension of 1 g of MNPs in 20 mL of distilled water was added to AG and MMT solutions and heated to 90 °C for 30 min. The solution condensed. This condensed solution was then poured into a Petri dish and solidified at room temperature. This solidified composite was placed in sunlight for complete drying. The same method was used for the preparation of 1 and 2% MMT (MNPs and AG) magnetic composite sheets. The summary of composites is given in Table 1.

Table 1. Composite Compositions

type	MNPs (g)	MMT (g)	AG (g)
0.5% MNPs (MMT and AG)	0.5	1	1
1.5% MNPs (MMT and AG)	1.5	1	1
2% MNPs (MMT and AG)	2	1	1
0.5% MMT (MNPs and AG)	1	0.5	1
1% MMT (MNPs and AG)	1	1	1
2% MMT (MNPs and AG)	1	2	1

2.6. Swelling Study. The swelling of composites was examined in distilled water. 0.1 g of each sample was allowed in 100 mL of distilled water for 24 h. The swelling ratio was measured by using eq 1.

$$\text{swelling ratio } (\%) = \frac{M2 - M1}{M1} \times 100 \quad (1)$$

$M1$ is the initial mass (g), and $M2$ is the final mass (g) of the composite.

2.7. Electrical Conductivity. A precision impedance analyzer (MICROTEST, 6630, Taiwan) and a 2401 Keithley SourceMeter Unit (SMU) were used for measuring electrical conductivity. Both instruments provided accurate measurements of the electrical properties of the tested materials.

2.8. Antibacterial Activity. The antibacterial activity of the synthesized MMT-based magnetic composite sheets was tested at a concentration of 100 μg/mL. AG media was prepared under sterilized conditions of a laminar flow hood. Composites were tested against *Escherichia coli* (strains were offered by the Department of Biochemistry, AWKUM). Zone of inhibition was measured in millimeters by using a caliper. Distilled water was taken as the negative control, while Ampicillin (5 μg/mL) was taken as the positive control.

2.9. Antioxidant Study. In this series of experiments, MMT-based magnetic composites were assessed for their antioxidant activity for DPPH (2,2-diphenylpicrylhydrazyl) at a concentration range of 12.5−200 μg/mL. Absorbance was measured at 517 nm using a spectrophotometer. Dose response curves were generated to calculate IC50 values.

3. RESULTS AND DISCUSSION

3.1. FTIR Analysis. The FTIR spectrum of the MNP (MMT and AG) magnetic composite was obtained in the wavenumber range from 400 to 4000 cm^{-1} and shown in Figure 1A. The characteristic bands correspond to different functional groups. The FTIR spectrum of 0.5% MNPs (MMT and AG), 1.5% MNPs (MMT and AG) and 2% MNPs (MMT and AG) exhibited the characteristic MNP bands at 573.66 cm^{-1} which reveal the Fe−O bending in MNPs. The Fe−OH group on the surface of MNPs shifted to Fe−O−Si due to the greater electronegativity of Si to the heightening of absorbance peaks at 604.25 cm^{-1}, which confirmed the presence of MMT clay. Peaks at 3383.94 and 1652.04 cm^{-1} correspond to HO stretching and bending. Peaks at 2980.14 and 2361.56 cm^{-1} correspond to alkyl asymmetric and symmetric CH_2 bending, which confirmed the presence of AG in the composite.[52] Similarly, the FTIR spectrum of 0.5, 1, and 2% MMT magnetic composites was taken in the wavenumber range from 400 to 4000 cm^{-1} and shown in Figure 1B. The characteristic bands correspond to different functional groups. The FTIR spectrum of 0.5, 1, and 2% MMT (MNPs and AG) magnetic composites exhibited the characteristic peaks at 2980.14 and 2361.56 cm^{-1} corresponding to the alkyl asymmetric and symmetric CH_2 bending, which confirmed the presence of AG and the smaller peaks at 573.66and 622.03 cm^{-1}, which reveal the Fe−O bending which confirmed the bonding of MNP nanoparticles with the MMT surface groups. The peaks at 3383.94 and 1652.04 cm^{-1} correspond to HO stretching and bending. The galactose bridge of AG units falls in the range of 900−1050 cm^{-1}.[53]

3.2. SEM Analysis. The texture and surface morphology of the various clay-based magnetic nanocomposite sheets were further evaluated by scanning electron microscopy (SEM). Figure 2 shows the various composite sheets of MMT and MNPs, i.e., 0.5 and 2%. As expected, AG has a smooth and nonporous surface with uniform morphology combined with the same concentration of MMT which becomes quite compact in structure and becomes open with a flake shape after sonication, and subsequently the incorporation of iron oxide nanoparticle morphology was significantly changed by the appearance of a rough and coarse surface. The 0.5% MNP (MMT and AG) micrograph shows the smooth texture and compact morphology, revealing the presence of AG and MMT, and the shiny appearance reveals the presence of iron oxide nanoparticles. In 2% MNPs (MMT,AG) MNP composite as the content of iron oxide increase in AG/MMT nanocomposite, the formation of homogeneously distributed MNPs sheet. MNPs are agglomerated and stuck to each other, thus making the surface bumpy and coarse.[53] 0.5 and 2% MMT metaphors specify that a greater dispersion of clay in the nanocomposite was acquired at a low degree of clay content less than 1 g, and perceptibly clay agglomerates were pragmatic with a higher degree of clay content more than 1 g. The presence of floc clumps suggested the poor dispersion of MNPs in MMT and AG.[54]

https://doi.org/10.1021/acsomega.3c08708
ACS Omega 2024, 9, 15904−15914

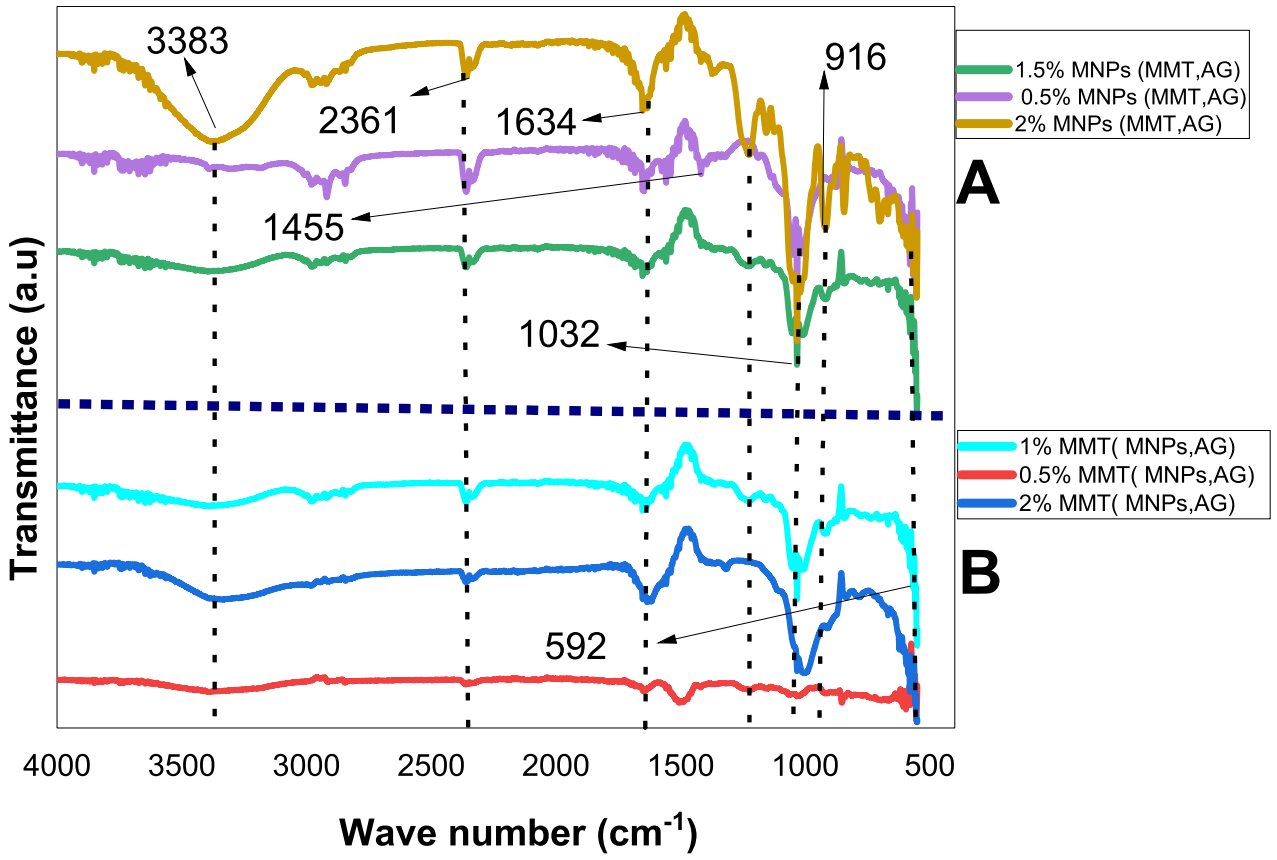

Figure 1. (A) Combined FT-IR spectra of 0.5, 1.5, and 2% MNP (MMT and AG) magnetic composites and (B) 0.5, 1, and 2% MMT (MNPs and AG) magnetic composites.

3.3. Thermal Analysis. TGA and DTA analyses of all the six samples are given in Figure 3A–D which were carried out under N_2 flow and heated from ambient temperature to 700 °C at 10 °C/min for various %Fe-based composites. TGA and DTA analyses give information about the molecular arrangements and organic fillings in the composite sheets. The TGA curve of the magnetic composite sheet has two distinct steps. The first step starts from 49 to 180 °C, i.e., 7% weight loss due to physiosorbed water molecules, at about 190 °C thermal decomposition, attributed to the degradation of galactose units. At 200–300 °C, the chemisorbed water and some gaseous content evaporate. This weight loss is probably due to the iron oxide present in the composite iron oxide nanoparticles showing very good thermal stability below 600 °C with irrelevant weight loss. The slight weight loss shown from 500 °C is due to the lattice OH groups with a weight loss of 20%, which corresponds to the exothermic peaks in DTA. The 2% MNP (MMT and AG) composite showed the stability to temperature as compared to 1.5% MNP (MMT and AG) and 0.5% MNP (MMT and AG) composites because of the greater weight loss.

Thermal analysis for various MMT-based magnetic composites, 0.5% MMT (MNPs and AG), 1% MMT (MNPs and AG), and 2% MMT (MNPs and AG) sheets gives information about the molecular arrangements and organic fillings in the composite sheets. Initially, they show stability to temperature because of the negligible weight loss up to 80 °C. The TGA curve of MMT-based magnetic composite sheet has two distinct steps. The first step starts from 50 to 180 °C with a weight loss between 5 and 7% related to the loss of absorbed moisture. The second step of weight loss is at about 280 °C, where a main thermal degradation of galactose units, release of SO_2, and fragmentation of AG carbohydrates start. Finally, a complete decomposition of AG occurred at 500 °C with a weight loss of 24% which corresponds to the exothermic peak at DTA.[53]

3.4. X-ray Diffraction Analysis. X-ray diffraction patterns of different percentages of MMT-based magnetic composite sheets are plotted in Figure 4. The incorporation of MMT and MNP nanoparticles in AG in order to form composite sheets is confirmed by XRD.

The XRD outlines of the prepared MNP (MMT and AG) composites presented the diffraction peaks at 2θ values of 28.656, 30.54, 36.00, 45.60, and 63.28; no other impurity-interrelated peaks were noticed. This confirmed the formation of magnetite nanoparticles, as shown in Figure 4B.[52] The XRD outlines of MNPs–AG nanoparticles presented that the crystalline structure is conserved after the layering of AG. According to the Scherrer equation, the MNP–AG nanoparticle crystal grain size is spherical.[53] Large filling sum of the MNPs in the composite sheets and the high crystalline nature of the MNPs deteriorated the comparative intensity of the diffraction peaks of MMT.[55]

The XRD results of 0.5, 1, and 2% MMT (MNPs and AG) magnetic composite sheets are shown in Figure 4A. The XRD patterns of the composite sheets presented the various diffraction peaks at 2θ values of 28.656, 30.54, 36.00, 45.60, and 61.992 as the characteristics peaks of MMT,[55] signifying the fruitful synthesis of MMT-based magnetic composites. Diffraction peaks could be allocated to the hexagonal structure

https://doi.org/10.1021/acsomega.3c08708
ACS Omega 2024, 9, 15904–15914

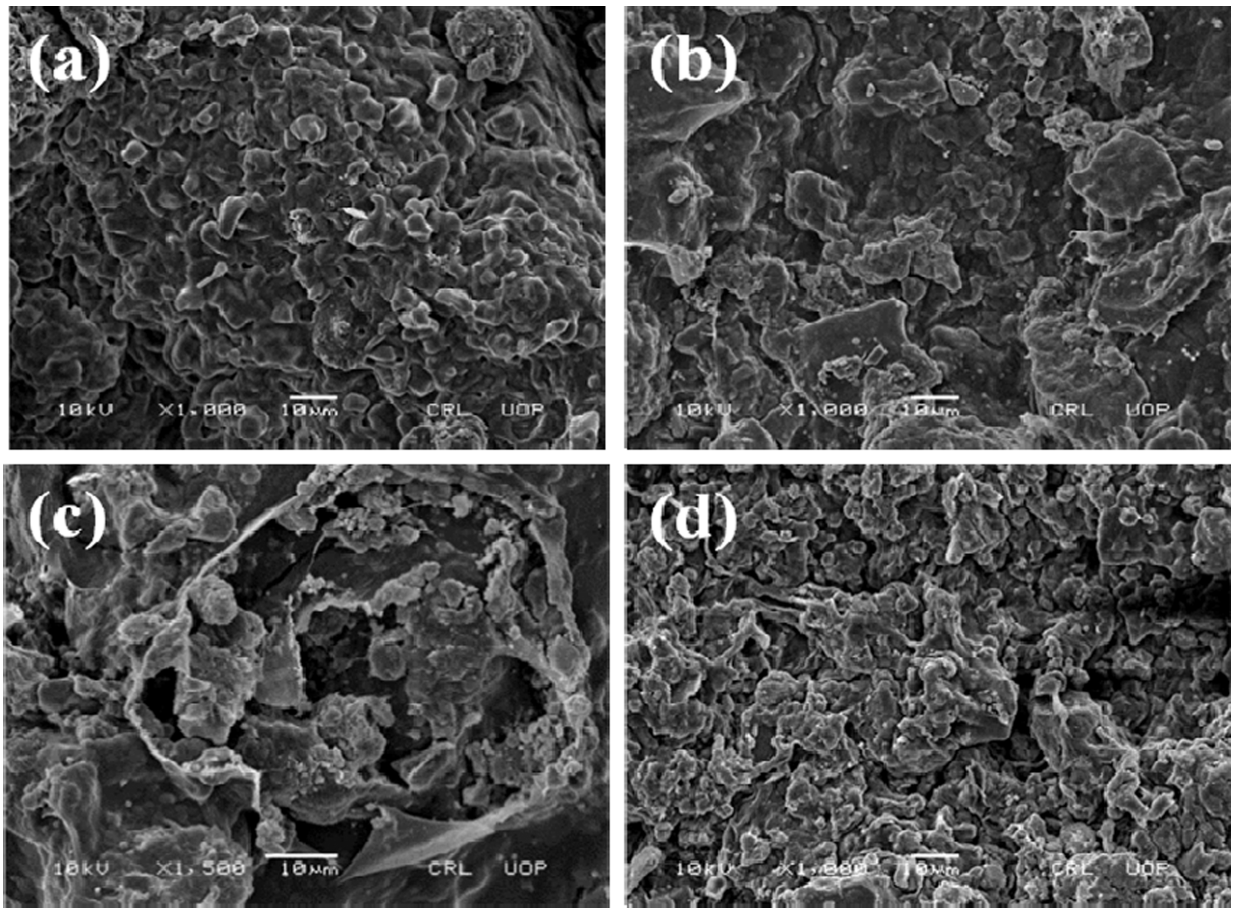

Figure 2. SEM micrographs of (a) 0.5% MNPs (MMT and AG), (b) 2% MNPs (MMT and AG), (c) 0.5% MMT (MNPs and AG), and (d) 2% MMT (MNPs and AG).

of MNPs (JCPDS Card 25-1402). Further, diffraction peaks seen at 26.6, 35.1, 45.4, and 61.9 are related to MMT. The XRD outline of MNPs is sharp and intense, suggesting a progressive degree of crystallinity. It offered that the filling of MMT can efficiently reduce the progression of the crystalline grain.[54]

3.5. Swelling Ratio (SR). The dry specimens were trimmed into square shapes, each weighing 0.1 g. To assess their swelling ratios, they were submerged in room-temperature water for a period of 24 h. Upon completion, the sample weights were recorded, and the swelling ratios were calculated accurately. The final data are given in Table 2.

Table 2 shows the swelling ratios of MMT-based magnetic composite sheets in water for 24 h at room temperature. Figure 5 clearly shows that the maximum swelling is obtained for composites containing fewer MNPs as compared to a higher content. This deviation in swelling ratio is due to the presence of more hydrophilic groups in the magnetic composite. The addition of more iron oxide (which is hydrophobic) into the MMT and AG magnetic composite reduces the number of hydrophilic groups in the composite which decreases the mutual action between water and hydrophilic groups of the composite. It is concluded that the internalization of hydrophilic or hydrophobic groups in the magnetic composite can manage the behavior of phase transition.[56] The primary factor influencing the extent of expansion in the composite is the specific exchangeable cation found within the MMT. Within the range of swelling, which encompasses the transitional phase between the crystalline and osmotic swelling, an MMT particle exhibits a behavior akin to a series of switches. As the interlayer spaces of the particle gradually absorb a specific quantity of water molecules, adjacent MMT layers undergo a substantial increase in distance, surpassing their initial separation by more than twice.[57]

3.6. Conductivity of the Prepared Composite Sheets. MNPs have excellent magnetic and electrical properties. When they are incorporated to polymers, they alter their thermal and electrical behavior.[58]

To comprehend the electrical properties of the prepared samples, an examination of their electrical conductivity at different frequencies is essential. Figure 6 demonstrates the variation of σ'_{ac} with frequency on a logarithmic scale. To investigate the possible conduction mechanism, electrical conductivity (σ'_{ac}) was analyzed at different frequencies on a logarithmic scale, as plotted in Figure 6. The correlated barrier hopping (CBH) model provides a framework for understanding our test results.[59] In this model, the conduction of carriers is caused by obstacles separating the localized sites. The charge localization in magnetic Fe_3O_4 causes the induction of polarization (ε', ε''). This charge localization corresponds at least to one p-electron that is released from the oxygen ion O^{2-} to be trapped by a neighboring iron ion Fe^{3+} according to Kramer's model.[60] The electron hopping mechanism was established between the Fe and O atoms. This evidence suggests that the electron, carrying charge, behaves like a small particle and shifts from one iron atom to

https://doi.org/10.1021/acsomega.3c08708
ACS Omega 2024, 9, 15904−15914

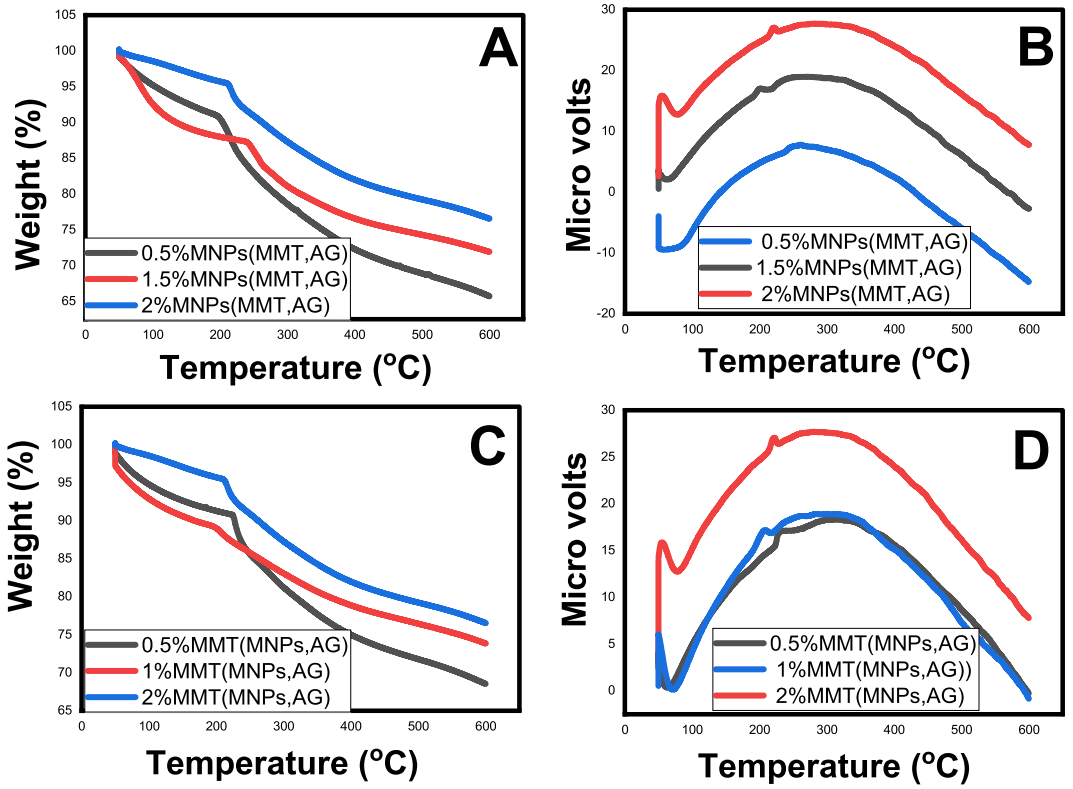

Figure 3. (A) TGA curves of various MNP (MMT and AG) magnetic composite sheets. (B) DTA curves of various MNP (MMT and AG) magnetic composite sheets. (C) TGA curves of various MMT (MNPs and AG) magnetic composite sheets. (D) DTA curves of various MMT (MNPs and AG) magnetic composite sheets.

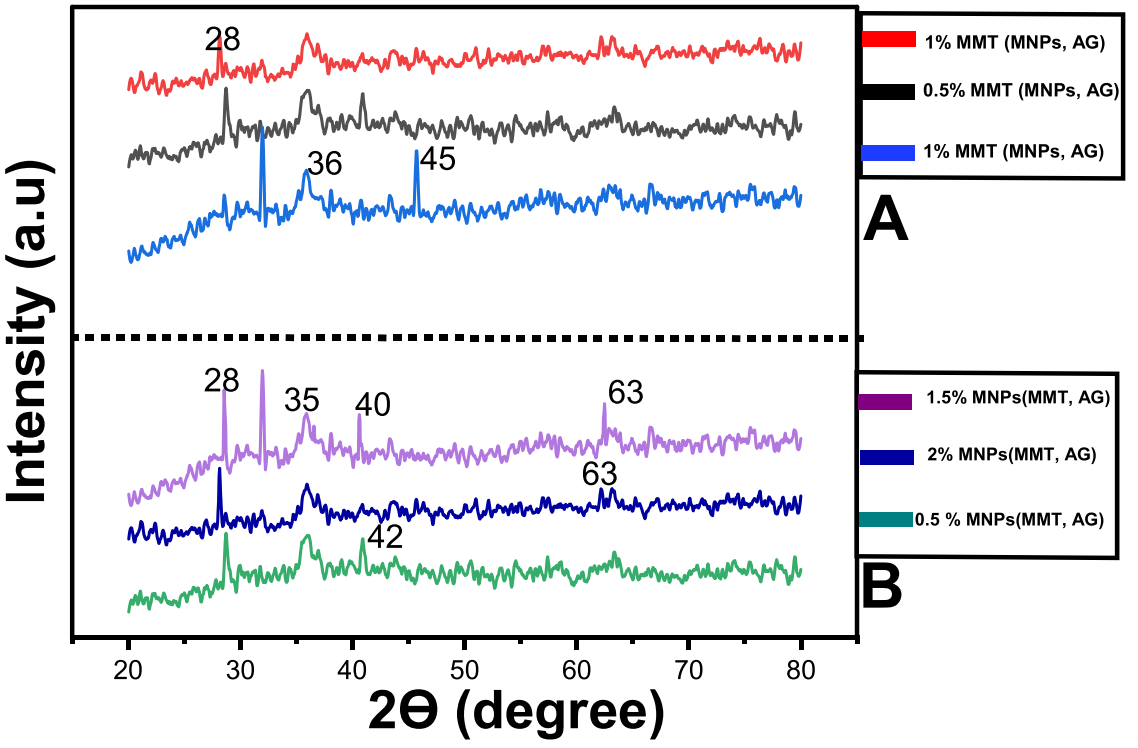

Figure 4. (A) XRD results of 0.5% MMT (MNPs and AG), 1% MMT (MNPs and AG), and 2% MMT (MNPs and AG). (B) XRD peaks of magnetic composites having different ratios of 0.5% MNPs (MMT and AG), 1.5% MNPs (MMT and AG), and 2% MNPs (MMT and AG).

another, leading to the conversion of Fe^{3+} to Fe^{2+} within the lattice.[61] Electricity predominantly flows on the exterior of the conductor, reaching a depth determined by the skin depth. The skin depth is determined by the rate at which the electric current oscillates. As the flow is faster, it tends to stay nearer to the surface and does not plunge as far down. Due to the skin

https://doi.org/10.1021/acsomega.3c08708
ACS Omega 2024, 9, 15904−15914

Table 2. Swelling Ratios of the Prepared Composite Sheets

sample	dry wt. (g)	swollen wt. (g)	water absorbed (g)	water (g) absorbed per gram of the sample	swelling ratio (%)
2% MNPs (MMT and AG)	0.1	0.43504	0.33504	3.3504	335.04
1.5% MNPs (MMT and AG)	0.1	1.0804	0.9804	9.804	980.4
0.5% MNPs (MMT and AG)	0.1	1.53127	1.43127	14.3127	1431.27
2% MMT (MNPs and AG)	0.1	1.83957	1.73957	17.3957	1739.57
1% MMT (MNPs and AG)	0.1	1.2804	1.1804	11.804	1180.4
0.5% MMT (MNPs and AG)	0.1	1.04106	0.94106	9.4106	941.06

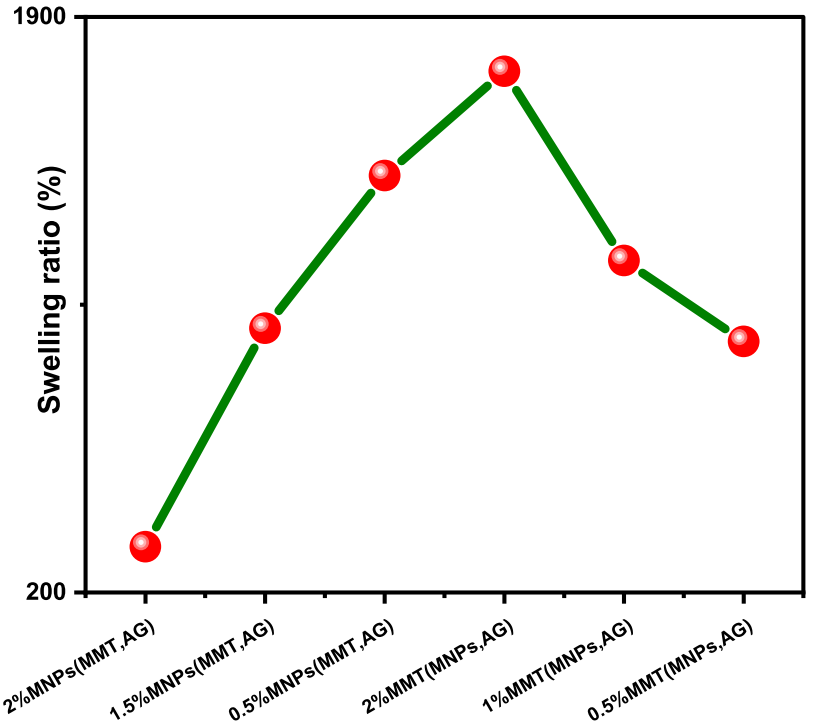

Figure 5. Swelling of various MMT (MNPs and AG) composites and MNP (MMT and AG) composites in dist. water.

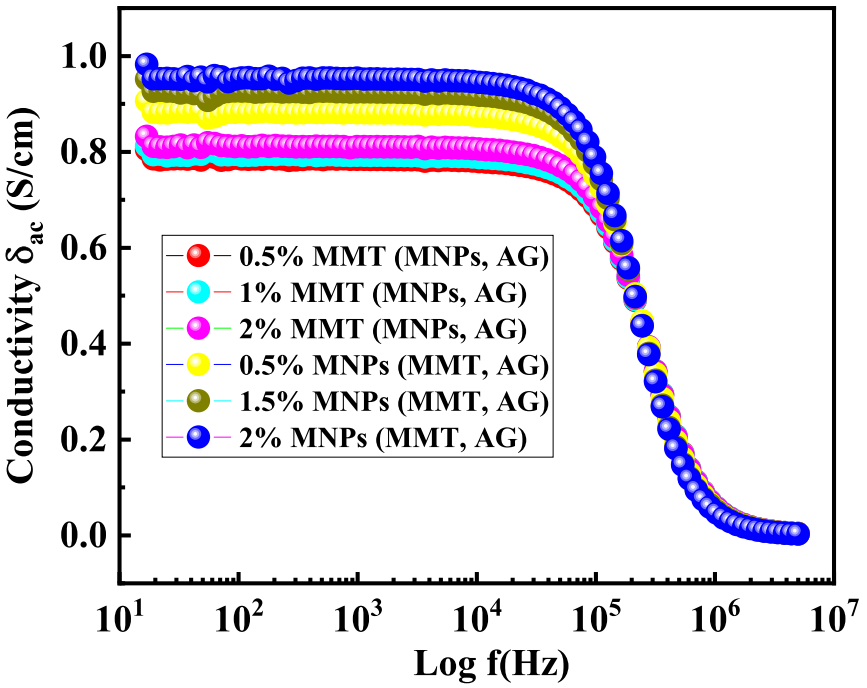

Figure 6. AC conductivity of various MMT (MNPs and AG) composites and MNP (MMT and AG) composites.

https://doi.org/10.1021/acsomega.3c08708
ACS Omega 2024, 9, 15904−15914

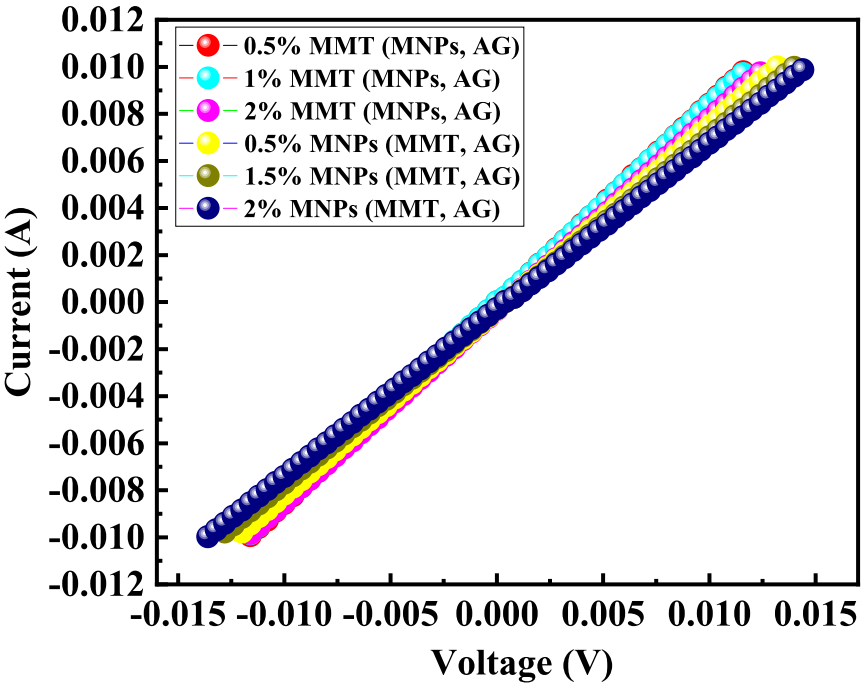

Figure 7. *I*–*V* characteristic curves of various MMT (MNPs and AG) composites and MNP (MMT and AG) composites.

effect, the electricity faces a higher level of resistance as it tries to pass through the conductor, as its effective cross section is diminished.[62] Figure 6 illustrates that as the frequency rises, the material's electrical conductivity decreases and exhibits characteristics similar to that of a conductor. According to Figure 7, the IV curves form straight lines, implying that the material exhibits characteristics of a metal conductor. The experiments were conducted at various voltage levels ranging from −0.0136 to +0.0136 V.

3.7. Antibacterial Activity. The antibacterial activity of the synthesized MMT-based magnetic composite sheets was tested against *E. coli*. AG media was prepared under the sterilized condition of laminar flow hood. *E. coli* smoothly struck on the surface of the media. Then, the composite was cut into small disks and placed on the surface of the media and incubated at 37 °C for 24 h. After 24 h, the zone of inhibition was measured and expressed in millimeters. The antibacterial activity on the MMT-based magnetic composite was tested on the aqueous solution of composite sheets of MNPs (MMT and AG) and MMT (MNPs and AG) against *E. coli*. The mean zone of inhabitation was determined after three trails of each composite sample and is shown in Table 3 and Figure 8. The

Table 3. Inhibition Zones of Various MMT (MNPs and AG) Composites and MNP (MMT and AG) Composites in Dist. Water

s.no	composite type	bacteria type	inhibition (mm)
1	0.5% MMT (MNPs and AG)	*E. coli*	10.67 ± 0.764
2	1% MMT (MNPs and AG)	*E. coli*	11 ± 0.764
3	2% MMT (MNPs and AG)	*E. coli*	7.93 ± 0.603
4	0.5% MNPs (MMT and AG)	*E. coli*	6.7 ± 0.361
5	1.5% MNPs (MMT and AG)	*E. coli*	8.7 ± 0.100
6	2% MNPs (MMT and AG)	*E. coli*	19 ± 0.300
7	Ampicillin	*E. coli*	27 ± 0.289
8	water	*E. coli*	0

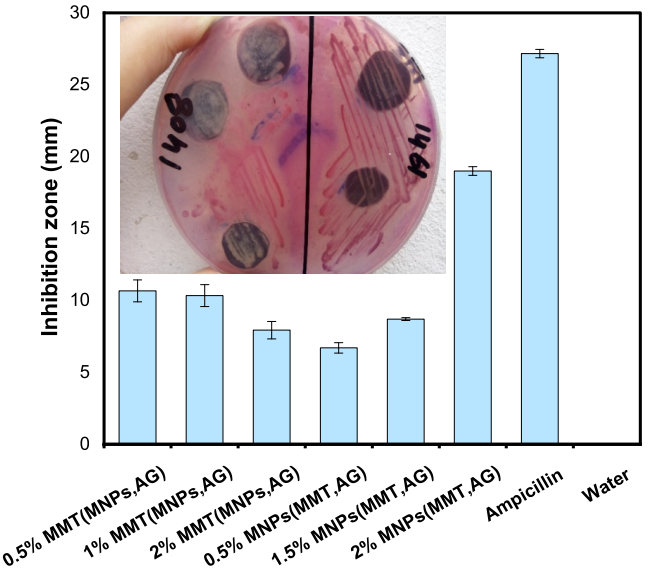

Figure 8. Inhibition zone against *E. coli* by various MMT (MNPs and AG) composites and MNP (MMT and AG) composites.

composites show zones of inhibition ranging from 6.7 to 19 mm. The antibacterial properties of MMT blend with MNPs have credited attraction by electrostatic forces of the negatively charged membrane of bacteria to the surface of clay on which positive Fe kills the bacteria.[63]

The physical and chemical properties of MMT make it a potential adsorbent for certain pathogens, such as bacteria and viruses. However, its effectiveness in removing all types of pathogens may be limited, particularly if they do not have a strong attraction to the surface of the clay.[64] The antibacterial effects of MNPs can be attributed to several key pathways, including the disruption of the bacterial cell membrane, production of reactive oxygen species (ROS), penetration of the membrane, and intracellular antibacterial effects involving

https://doi.org/10.1021/acsomega.3c08708
ACS Omega 2024, 9, 15904−15914

interaction with DNA and proteins. Metal oxides are formed through the bonding of metal ions with oxides, resulting in a densely packed structure.[65]

The load of metal NPs on the surface of MMT and its incorporation within the polymeric matrices and agar matrix cause a higher water uptake, proving the thermal stability and mechanical properties, along with changes in the barrier and permeability properties. Importantly, these composites exhibited improved antibacterial activity toward a broad variety of pathogens. Therefore, these materials are considered as potential active agents in food packaging, food bacteriology, agriculture, food technology, food preservation, clothing, and marine biofouling on ship.[66]

3.8. Antioxidant Activity. In this series of experiments, MMT-based magnetic composites were assessed for their antioxidant activity for DPPH (2,2-diphenylpicrylhydrazyl) at a concentration range of 12.5−200 μg/mL. Absorbance was measured at 517 nm using a spectrophotometer. Dose response curves were generated to calculate IC50 values which are shown in Table 4. According to data, an increase in concentration shows more activity in all composites. The absorbance value for these composites was also enhanced with an increase in concentration.

Table 4. IC50 Values of 1.5 and 2% MNPs (MMT and AG) and MMT (MNPs and AG) Magnetic Composites

composite type	IC50 value (μg/mL)
1.5% MNPs (MMT and AG)	46.55
2% MNPs (MMT and AG)	7.96
1% MMT (MNPs and AG)	46.55
2% MMT (MNPs and AG)	57.58

The absorbance value for 1.5% MNP (MMT and AG) composite at a concentration of 12.5−400 μg/mL was from 0.065 to 1.110, while the absorbance value for 2% MNP (MMT and AG) composite at the same concentration range was from 0.094 to 0.779. When their absorbance values were compared, it had been noticed that the 1.5% composite showed a high absorbance range as compared to the 2% composite sheet. From these dose response curves, IC50 values have been calculated. Data showed comparable activity of the magnetic composite with an IC50 value of (46.55) and (7.96), respectively. Both magnetic composites show comparable activity, as observed from the data from 1 and 2% MMT (MNPs and AG) magnetic composite. The absorbance value for 1% of MMT composite at a concentration of 12.5−400 μg/mL was from 0.065 to 1.110, while the absorbance value for 2% MMT magnetic composite at the same concentration range was from 0.153 to 0.940. When their absorbance values were compared, it had been shown that the 1.5% magnetic composite has a high absorbance range than the 2% composite sheet. From these dose response curves, IC50 values have been calculated, as listed in Table 4. Data showed comparable activity of the magnetic composite with IC50 values of (46.55) and (57.58), respectively. Both showed comparable activity.

4. CONCLUSIONS

In this study, a highly intercalated MMT-based magnetic composite was simply synthesized by the thermo-physicomechanical method. The prepared composite sheets were characterized by various techniques like SEM, XRD, TGA, DTA, and FTIR, and conductivity studies were also carried out and also checked for antibacterial and antioxidant tests. The SEM micrographs showed uniform dispersion of iron oxide nanoparticles and MMT in the magnetic composite, but the gradual increase of iron oxide nanoparticle content caused its agglomeration in the composite and lowering of its homogeneous distribution. The XRD pattern showed that the diffraction peak centered at 2-theta values of 30.33, 35.99, 43.99, 59.66, and 63.32°, which justified iron oxide incorporation in the composite. The results of TGA and DTA showed thermal stabilization of the prepared composites due to the addition of iron oxide. The FTIR spectra showed the characteristic peaks for MMT, iron oxide, and AG which confirm their presence in the composite sheets. Physical tests like swelling properties of the prepared composite sheets were done. It is concluded from the results that the introduction of iron oxide brought hydrophobic character to the composite. Antibacterial tests of the prepared composites were also investigated. The results made it clear that the composites have a meaningful inhibition over the growth of *E. coli* measured by disk diffusion. The composite also showed considerable antioxidant activity.

AUTHOR INFORMATION

Corresponding Author

Nasrullah Shah − *Department of Chemistry, Abdul Wali Khan University Mardan, Mardan KP-23200, Pakistan;* orcid.org/0000-0002-9125-0982; Email: nasrullah@awkum.edu.pk

Authors

Muffarih Shah − *Department of Chemistry, Abdul Wali Khan University Mardan, Mardan KP-23200, Pakistan;* orcid.org/0009-0005-7186-5663

Farishta Khan − *Department of Chemistry, Abdul Wali Khan University Mardan, Mardan KP-23200, Pakistan*

Touseef Rehan − *Department of Biochemistry, Women University Mardan, Mardan KP-23200, Pakistan*

Sulaiman Shams − *Department of Biochemistry, Abdul Wali Khan University Mardan, Mardan KP-23200, Pakistan*

Fatima Khitab − *Department of Chemistry, Shaheed Benazir Bhutto Women University, Peshawar KP-25000, Pakistan*

Abbas Khan − *Department of Chemistry, Abdul Wali Khan University Mardan, Mardan KP-23200, Pakistan*

Muhammad Wajid Ullah − *Biofuels Institute, School of the Environmental and Safety Engineering, Jiangsu University, Zhenjiang 212013, China*

Jasim Yousaf − *Department of Physics, Abdul Wali Khan University Mardan, Mardan KP-23200, Pakistan*

Fuad A. Awwad − *Department of Quantitative Analysis, College of Business Administration, King Saud University, Riyadh 11587, Saudi Arabia*

Emad A. A. Ismail − *Department of Quantitative Analysis, College of Business Administration, King Saud University, Riyadh 11587, Saudi Arabia*

Complete contact information is available at: https://pubs.acs.org/10.1021/acsomega.3c08708

Author Contributions

N.S.: conceptualization and supervision; M.S.: methodology and original draft writing; F.K.: reviewing final draft and software; T.R.: data collection and analysis; S.S.: experimental design and methodology; F.Kh.: literature review and method-

https://doi.org/10.1021/acsomega.3c08708
ACS Omega 2024, 9, 15904−15914

ology; A.K.: data interpretation; M.W.U.: experimental setup and data collection; J.Y.: electrical properties analysis; F.A.A.: statistical analysis, funding acquisition; E.A.A.I.: statistical analysis, funding acquisition.

Funding

This project was funded by King Saud University, Riyadh, Saudi Arabia

Notes

The authors declare no competing financial interest.

■ ACKNOWLEDGMENTS

Researchers Supporting Project number (RSPD2024R1060), King Saud University, Riyadh, Saudi Arabia.

■ REFERENCES

(1) Wang, Y.; et al. A novel AgNPs/sericin/agar film with enhanced mechanical property and antibacterial capability. *Molecules* **2018**, *23* (7), 1821.
(2) Nayak, K. K.; Gupta, P. In vitro biocompatibility study of keratin/agar scaffold for tissue engineering. *Int. J. Biol. Macromol.* **2015**, *81*, 1−10.
(3) Surendran, G.; Sherje, A. P. Biomedical Applications of Agar and its Composites: A Mini-Review. *Nat. Prod. J.* **2023**, *13* (5), 23−30.
(4) Long, J.; et al. Enzymatic preparation and potential applications of agar oligosaccharides: A review. *Critical Reviews in Food Science and Nutrition* **2022**, 1−17.
(5) Pandya, Y. H.; et al. Agar-Agar extraction, structural properties and applications: A review. *Pharma Innov. J.* **2022**, *11*, 1151−1157.
(6) Sousa, A. M.; Rocha, C.M.; Gonçalves, M. P. Agar. In *Handbook of hydrocolloids*; Elsevier, 2021; pp. 731−765.
(7) Salati, M. A.; et al. Agarose-based biomaterials: Opportunities and challenges in cartilage tissue engineering. *Polymers* **2020**, *12* (5), 1150.
(8) Basumatary, K.; et al. Lagerstroemia speciosa fruit-mediated synthesis of silver nanoparticles and its application as filler in agar based nanocomposite films for antimicrobial food packaging. *Food packaging and shelf life* **2018**, *17*, 99−106.
(9) Lee, H.; Rukmanikrishnan, B.; Lee, J. Rheological, morphological, mechanical, and water-barrier properties of agar/gellan gum/montmorillonite clay composite films. *Int. J. Biol. Macromol.* **2019**, *141*, 538−544.
(10) Theng, B. K. G. The Chemistry of Clay-Organic Reactions. In *The Chemistry of Clay-Organic Reactions*; Adam Hilger Ltd., Rank Precision Industries, 1974.
(11) Biswas, M.; Ray, S. S. Recent progress in synthesis and evaluation of polymer-montmorillonite nanocomposites. *New polymerization techniques and synthetic methodologies* **2001**, *155*, 167−221.
(12) Günister, E.; et al. Synthesis and characterization of chitosan-MMT biocomposite systems. *Carbohydr. Polym.* **2007**, *67* (3), 358−365.
(13) Shafei, L.; et al. Electronic Structure and Mechanical Properties of Solvated Montmorillonite Clay Using Large-Scale DFT Method. *Crystals* **2023**, *13* (7), 1120.
(14) Sadeghi, K.; Shahedi, M. Physical, mechanical, and antimicrobial properties of ethylene vinyl alcohol copolymer/chitosan/nano-ZnO (ECNZn) nanocomposite films incorporating glycerol plasticizer. *Journal of Food Measurement and Characterization* **2016**, *10*, 137−147.
(15) Srinivasan, S. Y.; et al. Magneto-conducting core/shell nanoparticles for biomedical applications. *ChemNanoMat* **2018**, *4* (2), 151−164.
(16) Sun, C.; Lee, J. S.; Zhang, M. Magnetic nanoparticles in MR imaging and drug delivery. *Advanced drug delivery reviews* **2008**, *60* (11), 1252−1265.
(17) Alavi, M.; Karimi, N. Ultrasound assisted-phytofabricated Fe3O4 NPs with antioxidant properties and antibacterial effects on growth, biofilm formation, and spreading ability of multidrug resistant bacteria. *Artificial Cells, Nanomedicine, and Biotechnology* **2019**, *47* (1), 2405−2423.
(18) Nguyen, M. D.; et al. Fe3O4 Nanoparticles: Structures, Synthesis, Magnetic Properties, Surface Functionalization, and Emerging Applications. *Applied Sciences* **2021**, *11* (23), 11301.
(19) Colombo, M.; et al. Biological applications of magnetic nanoparticles. *Chem. Soc. Rev.* **2012**, *41* (11), 4306−4334.
(20) Srinoi, P.; et al. Bimetallic nanoparticles: enhanced magnetic and optical properties for emerging biological applications. *Applied Sciences* **2018**, *8* (7), 1106.
(21) Aly, A. A.; et al. Friction and wear of polymer composites filled by nano-particles: a review. *World J. Nano Sci. Eng.* **2012**, *2* (01), 32.
(22) Triantafyllidis, K. S.; et al. Epoxy− clay fabric film composites with unprecedented oxygen-barrier properties. *Chem. Mater.* **2006**, *18* (18), 4393−4398.
(23) Zhou, C.-H.; et al. Preparation and functionality of clay-containing films. *J. Mater. Chem.* **2011**, *21* (39), 15132−15153.
(24) Polat, T. G.; Duman, O.; Tunc, S. Agar/κ-carrageenan/montmorillonite nanocomposite hydrogels for wound dressing applications. *Int. J. Biol. Macromol.* **2020**, *164*, 4591−4602.
(25) Wu, H.; Krifa, M.; Koo, J. H. Flame retardant polyamide 6/nanoclay/intumescent nanocomposite fibers through electrospinning. *Text. Res. J.* **2014**, *84* (10), 1106−1118.
(26) Paci, M.; Filippi, S.; Magagnini, P. Nanostructure development in nylon 6-Cloisite® 30B composites. Effects of the preparation conditions. *European polymer journal* **2010**, *46* (5), 838−853.
(27) Filippi, S.; et al. Structure and morphology of HDPE-g-MA/organoclay nanocomposites: Effects of the preparation procedures. *Eur. Polym. J.* **2008**, *44* (4), 987−1002.
(28) Rhim, J.-W. Effect of clay contents on mechanical and water vapor barrier properties of agar-based nanocomposite films. *Carbohydr. Polym.* **2011**, *86* (2), 691−699.
(29) Müller, A. J.; et al. Super-nucleation in nanocomposites and confinement effects on the crystallizable components within block copolymers, miktoarm star copolymers and nanocomposites. *Eur. Polym. J.* **2011**, *47* (4), 614−629.
(30) Sothornvit, R.; et al. Effect of clay content on the physical and antimicrobial properties of whey protein isolate/organo-clay composite films. *LWT-Food Science and Technology* **2010**, *43* (2), 279−284.
(31) Habiba, U.; et al. Adsorption and photocatalytic degradation of anionic dyes on Chitosan/PVA/Na−Titanate/TiO2 composites synthesized by solution casting method. *Carbohydr. Polym.* **2016**, *149*, 317−331.
(32) Quispe-Dominguez, R.; et al. Synthesis and characterization of MgAl-DBS LDH/PLA composite by sonication-assisted masterbatch (SAM) melt mixing method. *RSC Adv.* **2019**, *9* (2), 658−667.
(33) Arzac, A.; et al. Comparison of the Emulsion Mixing and In Situ Polymerization Techniques for Synthesis of Water-Borne Reduced Graphene Oxide/Polymer Composites: Advantages and Drawbacks. *Particle & Particle Systems Characterization* **2014**, *31* (1), 143−151.
(34) Sathish, T.; et al. Influence of compression molding process parameters in mechanical and tribological behavior of hybrid polymer matrix composites. *Polymers* **2021**, *13* (23), 4195.
(35) Rouison, D.; Sain, M.; Couturier, M. Resin transfer molding of natural fiber reinforced composites: cure simulation. *Composites science and technology* **2004**, *64* (5), 629−644.
(36) Cavallaro, G.; et al. Organic-nanoclay composite materials as removal agents for environmental decontamination. *RSC Adv.* **2019**, *9* (69), 40553−40564.
(37) Singh, K. R.; et al. Cerium oxide nanoparticles: properties, biosynthesis and biomedical application. *RSC Adv.* **2020**, *10* (45), 27194−27214.
(38) Pacheco, C. et al. Implantable and long-lasting drug delivery systems for cancer treatment. In *Long-acting drug delivery systems*; Elsevier, 2022; pp. 129−162.
(39) Rajagopal, R. A. Functionalized carbon nanomaterials for biomedical imaging. In *Functionalized Carbon Nanomaterials for Theranostic Applications*; Elsevier, 2023; pp. 353−380.

https://doi.org/10.1021/acsomega.3c08708
ACS Omega 2024, 9, 15904−15914

(40) Sothornvit, R.; Rhim, J.-W.; Hong, S.-I. Effect of nano-clay type on the physical and antimicrobial properties of whey protein isolate/clay composite films. *Journal of Food Engineering* **2009**, *91* (3), 468−473.
(41) Khashayary, S.; Aarabi, A. Evaluation of physico-mechanical and antifungal properties of gluten-based film incorporated with vanillin, salicylic acid, and montmorillonite (Cloisite 15A). *Food and Bioprocess Technology* **2021**, *14* (4), 665−678.
(42) Hosseini, S. N.; Pirsa, S.; Farzi, J. Biodegradable nano composite film based on modified starch-albumin/MgO; antibacterial, antioxidant and structural properties. *Polym. Test.* **2021**, *97*, No. 107182.
(43) Daraei, P.; et al. Novel thin film composite membrane fabricated by mixed matrix nanoclay/chitosan on PVDF microfiltration support: Preparation, characterization and performance in dye removal. *Journal of membrane science* **2013**, *436*, 97−108.
(44) Huang, Y.; et al. Reinforcement of polycaprolactone/chitosan with nanoclay and controlled release of curcumin for wound dressing. *ACS omega* **2019**, *4* (27), 22292−22301.
(45) Ambre, A. H.; Katti, K.S.; Katti, D.R. Nanoclay based composite scaffolds for bone tissue engineering applications. *J. Nanotechnol. Eng. Med.* **2010**, *1*, No. 031013, DOI: 10.1115/1.4002149.
(46) Rani, P.; Ahamed, M. B.; Deshmukh, K. Significantly enhanced electromagnetic interference shielding effectiveness of montmorillonite nanoclay and copper oxide nanoparticles based polyvinylchloride nanocomposites. *Polym. Test.* **2020**, *91*, No. 106744.
(47) Xin, Y.; et al. Flexible piezoelectric sensor based on PVDF-TrFE/Nanoclay composite nanofibers for physiological micro-vibration signal sensing. *Measurement* **2022**, *201*, No. 111742.
(48) Klangmuang, P.; Sothornvit, R. Combination of beeswax and nanoclay on barriers, sorption isotherm and mechanical properties of hydroxypropyl methylcellulose-based composite films. *LWT-Food Science and Technology* **2016**, *65*, 222−227.
(49) Samanta, R. Recent Trends in Nanometric Dispersed Polymer Composites. In *Polymer Nanocomposites*; CRC Press, 2023; pp. 109−120.
(50) Gupta, A. K.; Gupta, M. Synthesis and surface engineering of iron oxide nanoparticles for biomedical applications. *biomaterials* **2005**, *26* (18), 3995−4021.
(51) Trang, V. T.; et al. Functional Iron Oxide−Silver Hetero-Nanocomposites: Controlled Synthesis and Antibacterial Activity. *J. Electron. Mater.* **2017**, *46* (6), 3381−3389.
(52) Ramasubbu, A.; Saravanan, S.; Vasanthkumar, S. One-pot synthesis and characterization of biopolymer−Iron oxide nanocomposite. *Int. J. Nano Dim.* **2011**, *2* (2), 105−110.
(53) Díaz-Bleis, D.; et al. On the preparation and characterization of superparamagnetic nanoparticles with Gelidium robustum agar coating for biomedical applications. *Bull. Mater. Sci.* **2018**, *41* (2), 39.
(54) Wang, J.; et al. Synthesis, characterization and photocatalytic activity of inexpensive and non-toxic Fe2O3− Fe3O4 nanocomposites supported by montmorillonite and modified by graphene. *Composites Part B: Engineering* **2017**, *114*, 211−222.
(55) Zhang, H.; et al. Nano γ-Fe2O3/bentonite magnetic composites: synthesis, characterization and application as adsorbents. *J. Alloys Compd.* **2016**, *688*, 1019−1027.
(56) Rhim, J. W.; Lee, S. B.; Hong, S. I. Preparation and characterization of agar/clay nanocomposite films: the effect of clay type. *J. Food Sci.* **2011**, *76* (3), N40−N48.
(57) Meleshyn, A.; Bunnenberg, C. The gap between crystalline and osmotic swelling of Na-montmorillonite: A Monte Carlo study. *J. Chem. Phys.* **2005**, *122* (3), No. 034705, DOI: 10.1063/1.1834499.
(58) Umare, S.; Shambharkar, B.; Ningthoujam, R. Synthesis and characterization of polyaniline−Fe3O4 nanocomposite: Electrical conductivity, magnetic, electrochemical studies. *Synth. Met.* **2010**, *160* (17−18), 1815−1821.
(59) Jonscher, A. K. Frequency-dependence of conductivity in hopping systems. *J. Non-Cryst. Solids* **1972**, *8*, 293−315.
(60) Kramers, H. J. P. L'interaction entre les atomes magnétogènes dans un cristal paramagnétique. *Physica* **1934**, *1* (1−6), 182−192.
(61) Rosso, K. M.; Smith, D. M.; Dupuis, M. An ab initio model of electron transport in hematite (α-Fe 2 O 3) basal planes. *J. Chem. Phys.* **2003**, *118* (14), 6455−6466.
(62) Silvester, P.J.P.O.T.I. *Modal network theory of skin effect in flat conductors.* **1966**, *54* (9), 1147−1151.
(63) Magana, S.; et al. Antibacterial activity of montmorillonites modified with silver. *J. Mol. Catal. A: Chem.* **2008**, *281* (1−2), 192−199.
(64) Mokhtar, A.; et al. Recent Advances in Antibacterial Metallic Species Supported on Montmorillonite Clay Mineral: A Review. *Minerals* **2023**, *13* (10), 1268.
(65) Kotrange, H.; Najda, A.; et al. Metal and Metal Oxide Nanoparticle as a Novel Antibiotic Carrier for the Direct Delivery of Antibiotics. *Int. J. Mol. Sci.* **2021**, *22*, 9596.
(66) Hossain, S. I.; et al. A Review on Montmorillonite-Based Nanoantimicrobials: State of the Art. *Nanomaterials* **2023**, *13* (5), 848.

https://doi.org/10.1021/acsomega.3c08708
ACS Omega 2024, 9, 15904−15914